Vinculin potentiates E-cadherin mechanosensing and is recruited to actin-anchored sites within adherens junctions in a myosin II–dependent manner

Quint le Duc,[1] Quanming Shi,[2] Iris Blonk,[1] Arnoud Sonnenberg,[5] Ning Wang,[3] Deborah Leckband,[2,4] and Johan de Rooij[1]

[1]Hubrecht Institute, University Medical Centre Utrecht, 3584 CT Utrecht, Netherlands
[2]Department of Chemical and Biomolecular Engineering, [3]Department of Mechanical Science and Engineering, and [4]Department of Chemistry, University of Illinois at Urbana-Champaign, Champaign, IL 61801
[5]Division of Cell Biology, The Netherlands Cancer Institute, 1066 CX Amsterdam, Netherlands

Cell surface receptors integrate chemical and mechanical cues to regulate a wide range of biological processes. Integrin complexes are the mechanotransducers between the extracellular matrix and the actomyosin cytoskeleton. By analogy, cadherin complexes may function as mechanosensors at cell–cell junctions, but this capacity of cadherins has not been directly demonstrated. Furthermore, the molecular composition of the link between E-cadherin and actin, which is needed to sustain such a function, is unresolved. In this study, we describe nanomechanical measurements demonstrating that E-cadherin complexes are functional mechanosensors that transmit force between F-actin and E-cadherin. Imaging experiments reveal that intercellular forces coincide with vinculin accumulation at actin-anchored cadherin adhesions, and nanomechanical measurements show that vinculin potentiates the E-cadherin mechanosensory response. These investigations directly demonstrate the mechanosensory capacity of the E-cadherin complex and identify a novel function for vinculin at cell–cell junctions. These findings have implications for barrier function, morphogenesis, cell migration, and invasion and may extend to all soft tissues in which classical cadherins regulate cell–cell adhesion.

Introduction

Cell surface receptors integrate both chemical and mechanical cues to regulate biological processes as diverse as differentiation, vascular development, tumor growth, and malignancy (Bershadsky et al., 2003; Discher et al., 2005; Vogel and Sheetz, 2006; Lecuit and Lenne, 2007; Kumar and Weaver, 2009). Integrin-based adhesion complexes are sensors of force between the ECM and the contractile actomyosin cytoskeleton (Bershadsky et al., 2003). Direct assays for integrin mechanosensing apply external force to ligand-coated beads bound to the cell surface and determine force-dependent reinforcement (or force-induced cell stiffening) from the reduction in bead displacement upon prolonged application of force (Wang et al., 1993; Choquet et al., 1997). Talin and vinculin are strongly implicated in this mechanoresponse (Giannone et al., 2003). In vitro force-dependent unfolding of talin opens up binding sites for vinculin (del Rio et al., 2009). In intact cells, recruitment of vinculin to tensile focal adhesions (FAs) is mediated by paxillin rather than direct talin binding (Pasapera et al., 2010). Overexpressing vinculin deletion mutants uncouples integrin-mediated adhesion from its regulation by cytoskeletal force (Humphries et al., 2007), and the absence of vinculin reduces cell stiffness (Mierke et al., 2008).

During morphogenesis, contractile forces at intercellular junctions direct cell patterning, drive convergence and extension

Q. le Duc and Q. Shi contributed equally to this paper.

Correspondence to Ning Wang: nwangrw@illinois.edu; Deborah Leckband: leckband@illinois.edu; or Johan de Rooij: j.derooij@hubrecht.eu

N. Wang, D. Leckband, and J. de Rooij contributed equally to this paper.

Abbreviations used in this paper: COMP, cartilage oligomerizing protein; CSK, cytoskeleton preserving; FA, focal adhesion; FRET, fluorescence resonance energy transfer; HGF, hepatocyte growth factor; IF, immunofluorescence; IP, immunoprecipitation; ko, knockout; MTC, magnetic twisting cytometry; pMLC, phosphorylated myosin light chain; ROI, region of interest; TIRF, total internal reflection fluorescence; wt, wild type.

The Rockefeller University Press $30.00
J. Cell Biol. Vol. 189 No. 7 1107–1115
www.jcb.org/cgi/doi/10.1083/jcb.201001149

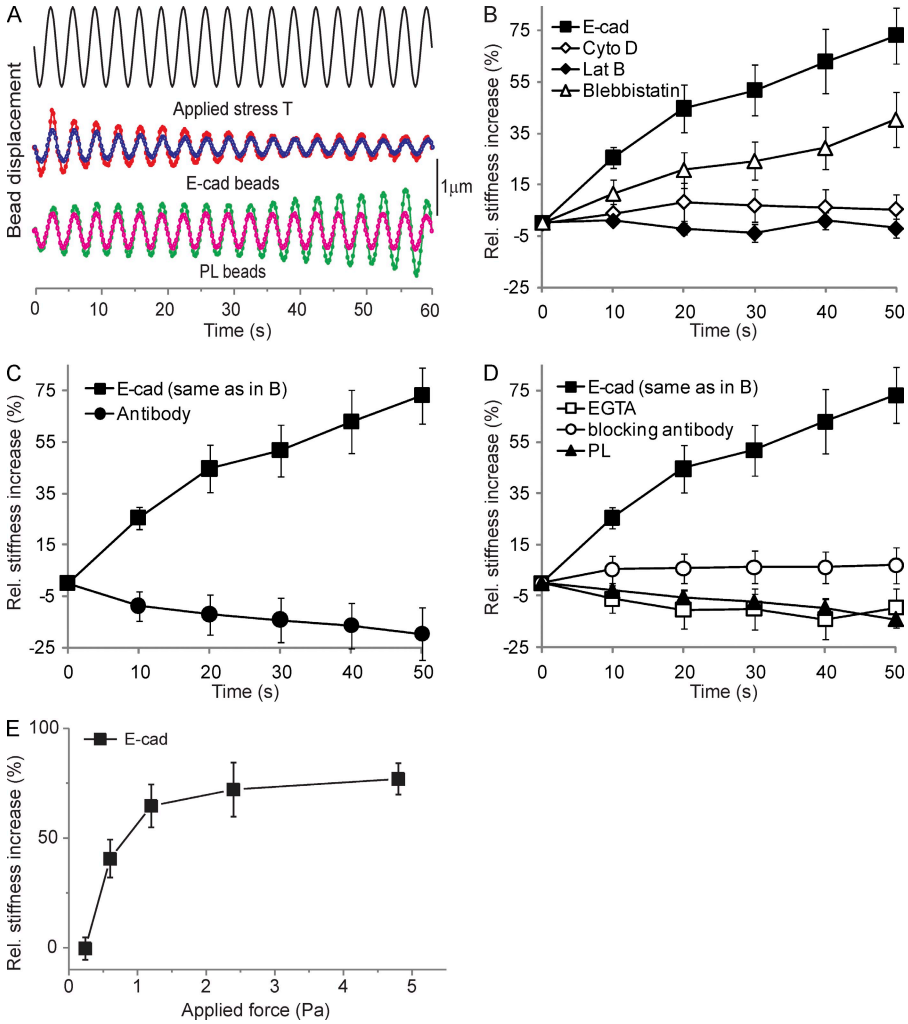

Figure 1. **E-cadherin is a mechanosensor.** (A) Continuous driving field modulation at 0.3 Hz for 60 s (2.4 Pa stress) and representative time course of the displacement of two E-cadherin– and poly-L-lysine (PL)–coated beads. (B) The force-induced stiffening of Fc–E-cadherin–coated beads relative to unperturbed bead–cell contacts in the absence (E-cad) or presence of latrunculin B (Lat B), cytochalasin D (Cyto D), or blebbistatin. (C) Fc–E-cadherin–coated beads versus beads coated with monoclonal E-cadherin antibody. (D) Fc–E-cadherin–coated beads in the absence or presence of 3 mM EGTA added just before MTC or blocking anti–E-cadherin antibody versus beads coated with poly-L-lysine. (E) The percent change in E-cadherin junction stiffness relative to unperturbed cells as a function of applied shear stress is shown. After 20 min of bead–cell contact, the beads were subjected to a modulated 0.3-Hz magnetic field for 60 s. The elastic shear modulus was determined at 50 s as a function of the amplitude of the applied shear stress. (B–E) Each data point represents >300 beads. Error bars represent SD.

movements, and regulate germ cell migration (Lecuit, 2005; Kardash et al., 2010). Also, endothelial cells coordinately align with shear flow (Tzima et al., 2005). Classical cadherins are good candidates for mechanosensing at cell–cell junctions. Myosin II activity is required for accumulation and stability of cadherins at junctions (Shewan et al., 2005; Miyake et al., 2006; Lambert et al., 2007). However, actomyosin contraction disrupts epithelial cell–cell adhesion in response to hepatocyte growth factor (HGF; de Rooij et al., 2005) or oncogenes such as Ras and Src (Zhong et al., 1997; Krendel et al., 1999; Avizienyte et al., 2004; Ayollo et al., 2009). The defining characteristic of mechanosensors is the capacity to both sense force and generate a proportional cell response (Vogel and Sheetz, 2006). As none of the prior investigations actually probed forces to demonstrate this, direct evidence for mechanosensing by cadherins is lacking (Schwartz and DeSimone, 2008). Moreover, the existence of a mechanical link between the E-cadherin complex and cytoskeleton, a necessity for mechanosensing, was challenged by recent findings (Drees et al., 2005; Yamada et al., 2005).

In this study, we present direct evidence that the E-cadherin complex is a mechanosensor that probes the mechanical environment to elicit a proportional change in the mechanics of the junctions. Furthermore, we show that vinculin potentiates E-cadherin–mediated mechanosensing and localizes to tension-bearing sites in cell–cell junctions to mediate mechanoregulation of cell–cell adhesion.

Results and discussion

The E-cadherin complex is a mechanosensor

We used magnetic twisting cytometry (MTC; Fig. 1 A; Wang and Ingber, 1995) to test whether mechanical stimulation affects the viscoelastic properties of junctions between F9 cells and Fc–E-cadherin–coated beads. All measurements were performed after 20 min of bead–cell contact to resolve force-dependent from force-independent changes in stiffening, which plateaus after ~15 min (see Fig. 4 B). During continuous shear modulation, bead displacement amplitude decreased with the forcing time (Fig. 1 A), amounting to a force-actuated 70% increase in stiffness, which is relative to previously unperturbed cells (Fig. 1 B). Latrunculin B, cytochalasin D, and blebbistatin strongly affected this response, demonstrating that cadherin force transmission requires a direct mechanical link to an organized and contractile actin cytoskeleton.

Beads coated with an anti–E-cadherin antibody bound strongly to the cell surface but did not display any force-actuated stiffening (Fig. 1 C). Moreover, addition of EGTA or an

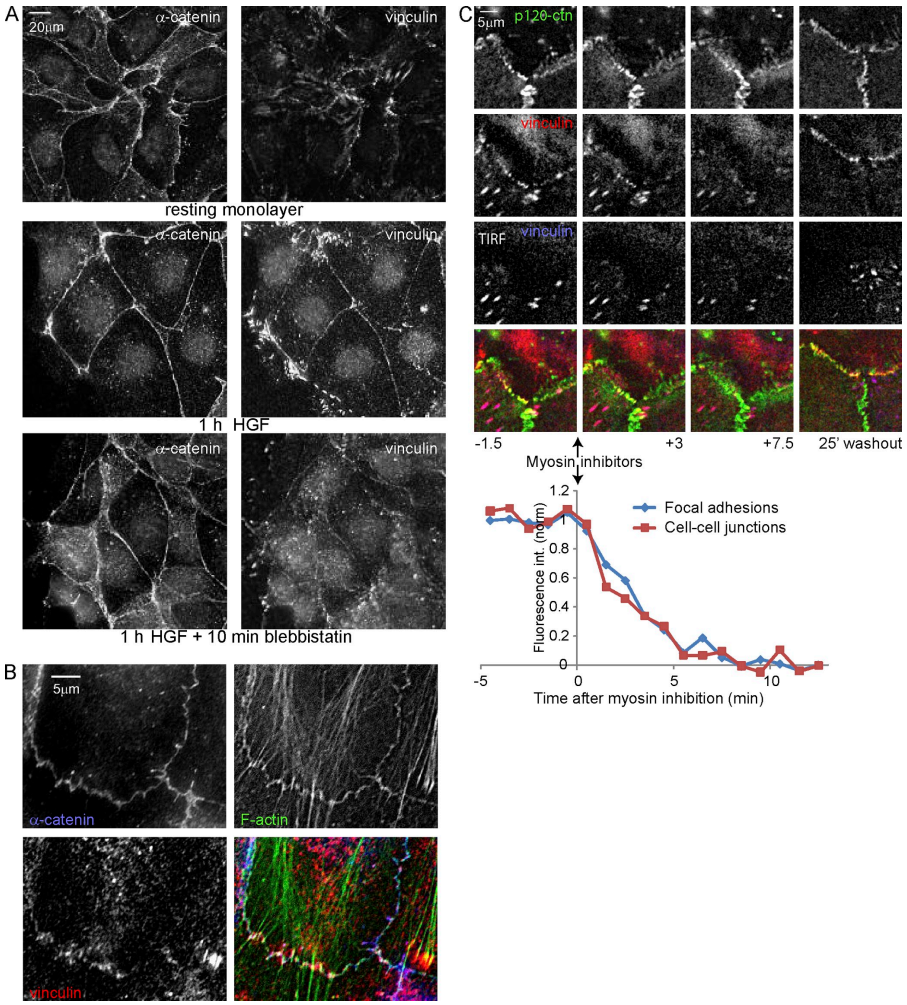

Figure 2. **Vinculin is recruited to active cell–cell junctions in a myosin-dependent manner.** (A) IF after CSK buffer extraction shows HGF-induced and myosin II–dependent α-catenin and vinculin distribution. (B) Magnified view of vinculin in cell–cell junctions of HGF-stimulated cells. (C) Cells expressing EGFP-vinculin (stably) and mCherry–p120-catenin (p120-ctn; transiently) analyzed by widefield and TIRF microscopy 1 h after HGF treatment. 3 µM ML-7 and 10 µM Y27632 were added 15 min after the start of imaging and washed out after another 10 min. EGFP-vinculin fluorescence intensity was measured in FAs (15 ROIs, each containing two to four FAs from seven time lapses) and cell–cell contacts (eight ROIs from seven time lapses).

E-cadherin–blocking antibody after 20 min of Fc–E-cadherin bead–cell contact just before the MTC measurements completely abolished the force-actuated stiffening (Fig. 1 D). Finally, poly-L-lysine–coated beads showed no stiffening (Fig. 1, A and D). This argues that contaminating integrin–bead contacts (because of nonspecific protein adsorption to beads) are not affecting our results and demonstrates that specific cadherin ligation is required. This is similar to integrins (Choquet et al., 1997) and highlights the importance of using proper ligands to elicit the mechanoresponse.

Finally, the relative stiffness increase at cadherin junctions increases with the applied bond shear up to a limiting plateau at stresses >2 Pa (Fig. 1 E). This increase in junction stiffness in proportion to the applied stress ultimately confirms that E-cadherin complexes are bona fide mechanosensors. Although regulation of E-cadherin complexes by contractile force is suggested by the myosin II requirement, direct evidence for force-dependent reinforcement of E-cadherin adhesions had not been presented to our knowledge. Thus, our data show for the first time that the E-cadherin complex is a mechanosensor.

Myosin-dependent recruitment of vinculin to active cell–cell junctions

We investigated the localization of putative cadherin–actin linker proteins after HGF stimulation, which increases tension on cell–cell junctions (see Fig. 5 A; de Rooij et al., 2005). As shown in Fig. 2 A and Fig. S1, E-cadherin, α-, β-, p120-catenin, and EPLIN (Abe and Takeichi, 2008) are localized at similar levels in steady-state and HGF-stimulated cell–cell adhesions. Interestingly, vinculin scarcely localizes to steady-state cell–cell adhesions, whereas its colocalization with α-catenin is much more evident in junctions after HGF (Fig. 2 A). Treatment with blebbistatin for 10 min largely abolished vinculin localization to cell–cell junctions, suggesting that this localization is indeed tension dependent. We conclude that vinculin is recruited to cell–cell junctions in a myosin II–dependent manner.

Closer analysis of Fig. 2 B shows that vinculin does not colocalize with the E-cadherin complex all over cell–cell junctions but is restricted to those sites in which junctions contact F-actin bundles and, thus, likely experience increased tension. Moreover, dual-color imaging of GFP-vinculin and mCherry–p120-catenin shows that cell spreading induced by HGF is followed by an increase in contraction, which marks the onset of vinculin accumulation at discrete sites within cell–cell junctions (Video 1). Finally, Fig. 2 C and Video 2 show that EGFP-vinculin, but not mCherry–p120-catenin, rapidly disappears from cell–cell junctions when tension is relieved by inhibitors. Upon inhibitor washout, tension is restored concomitant with a relocalization of vinculin to cell–cell junctions (Fig. 2 C and Video 2). Quantification

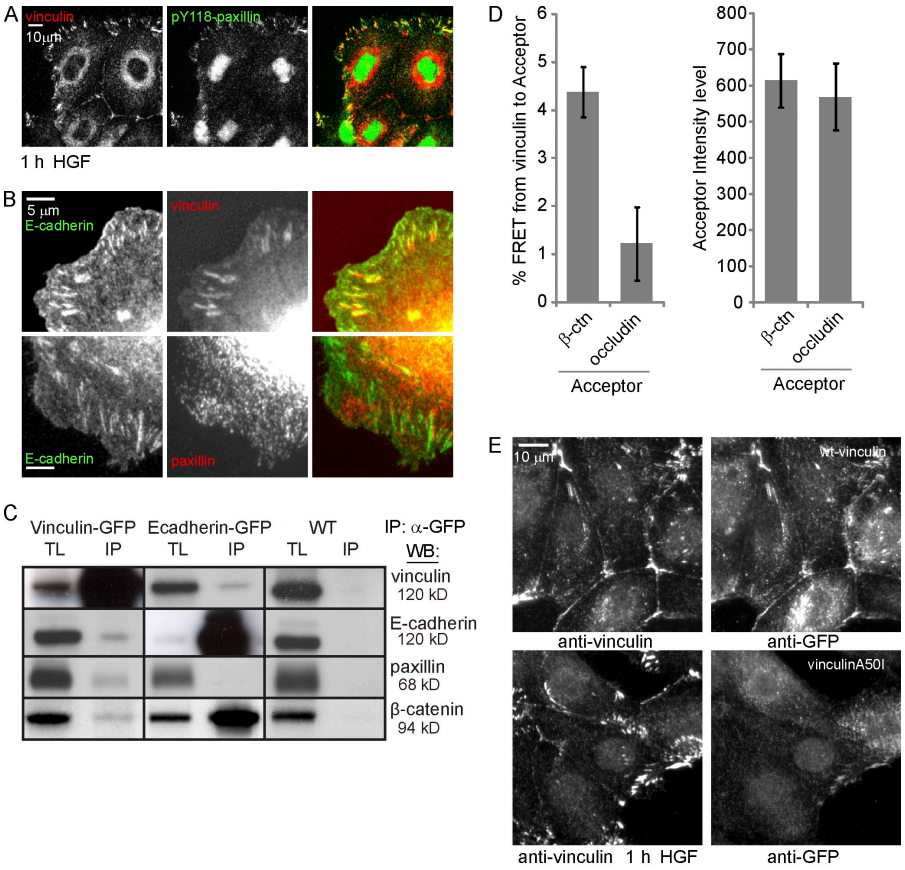

Figure 3. **Vinculin closely interacts with the E-cadherin complex.** (A) Recruitment of vinculin but not pY118-paxillin to cell–cell junctions in HGF-stimulated cells shown by IF. (B) Colocalization of vinculin but not paxillin with GFP–E-cadherin in E-cadherin–COMP adhesions revealed by IF. (C) Western blot (WB) analyses of total lysates (TL) and IP of endogenous E-cadherin, vinculin, paxillin, and β-catenin co-IP with GFP-tagged vinculin or E-cadherin from cell lysates after cross-linking. Black lines indicate that intervening lanes have been spliced out. (D, left) FRET from immunolabeled GFP-vinculin (Alexa Fluor 488) to immunolabeled β-catenin (β-ctn) or occludin (rhodamine). Error bars represent SEM (n = 18). (right) Mean acceptor fluorescence intensity in the ROIs used for calculating FRET. (E) MDCK cells transfected with GFP-vinculin or GFP–vinculin A50I were washed with CSK buffer, fixed, and immunostained for vinculin and GFP simultaneously.

of the EGFP-vinculin intensity shows that the loss of vinculin from cell–cell junctions upon myosin inhibition follows the same time curve as the loss of vinculin from FAs. We conclude that during activation of cell–cell adhesions by HGF, a pool of vinculin accumulates at discrete, actin-anchored sites in cell–cell junctions, which is concurrent with increased myosin II–dependent tension.

Vinculin interacts with the E-cadherin complex at cell–cell junctions

Total internal reflection fluorescence (TIRF) microscopy (Fig. 2 C and Video 2) shows that the pool of vinculin in cell–cell junctions is distinct from the vinculin in FAs. Furthermore, the FA protein paxillin does not colocalize with vinculin at cell–cell contacts after HGF (Video 3). Finally, tyrosine-118–phosphorylated (pY118) paxillin, which mediates myosin II–dependent recruitment of vinculin to FAs (Pasapera et al., 2010), shows no colocalization with the cell–cell junction pool of vinculin (Fig. 3 A). Thus, we conclude that vinculin is recruited to cell–cell junction complexes, which do not contact the basal ECM, through intermediates that are distinct from those that mediate recruitment of vinculin to FAs.

To separate E-cadherin adhesions from other cell–cell adhesion complexes, we plated MDCK cells on coverslips coated with E-cadherin–cartilage oligomerizing protein (COMP), a pentamerizing fusion of the ectodomain of E-cadherin and COMP (Tomschy et al., 1996), to induce the formation of actin-anchored E-cadherin adhesions (Fig. S1 A). These E-cadherin–COMP adhesions contain E-cadherin (Fig. 3 B) and α-, β-, and p120-catenin (Fig. S2, A and F) but not proteins found at other types of cell–cell junctions (nectin and claudin; Fig. S2 F) or FAs (paxillin; Fig. 3 B). Furthermore, they depend on actomyosin activity and calcium (Fig. S2, B and C) and are insensitive to blocking antibodies to β1- and α6-integrins, which mediate basal ECM adhesion in MDCK cells (Fig. S2, D and E). The fact that vinculin strongly localizes to E-cadherin–COMP adhesions (Fig. 3 B) leads to the conclusion that vinculin is recruited to the E-cadherin complex that forms a direct and functional interaction with actomyosin in cells on E-cadherin–COMP.

In immunoprecipitation (IP) after reversible chemical cross-linking followed by boiling and trituration of insoluble material that includes the cell–cell junctions (Hinck et al., 1994), endogenous vinculin precipitates with GFP–E-cadherin, and endogenous E-cadherin precipitates with GFP-vinculin (Fig. 3 C). Compared with total protein levels, β-catenin more efficiently precipitates with E-cadherin, whereas paxillin more efficiently precipitates with vinculin. We could not reproduce the efficient co-IP of vinculin and E-cadherin observed in other cell lines (Hazan et al., 1997; Maddugoda et al., 2007; Peng et al., 2010). Nevertheless, the inefficient co-IP of vinculin and E-cadherin from MDCK cells correlates well with the low abundance of vinculin in their cell–cell adhesions observed by fluorescence (Figs. 2 and 3). Thus, E-cadherin and vinculin reside in one complex, which, in MDCK cells, is not very abundant compared with other complexes in which these proteins reside. The amount of coprecipitated E-cadherin and vinculin

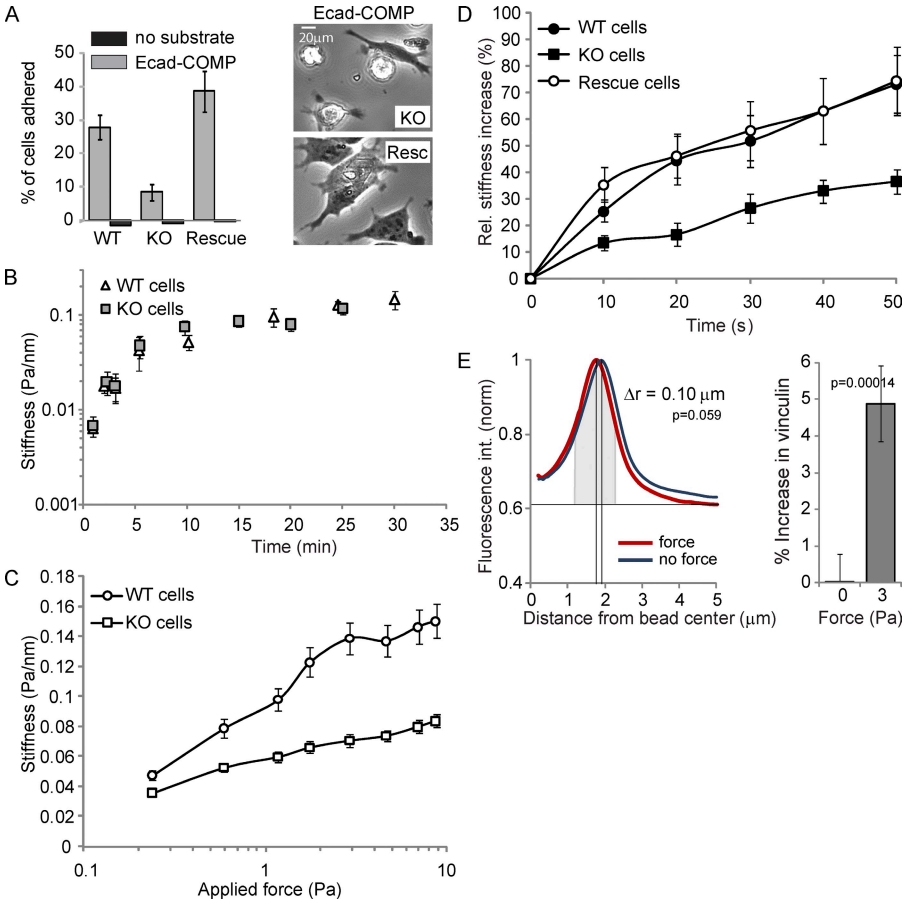

Figure 4. **Vinculin modulates E-cadherin mechanosensing.** (A, left) The relative number of wt, ko, and vinculin-reconstituted F9 cells that adhered to E-cadherin–COMP-coated wells after 45 min is shown. (right) Phase-contrast images of ko and reconstituted cells on E-cadherin–COMP. (B) The force-independent stiffening of E-cadherin junctions as a function of the bead–cell contact time. After increasing periods of bead–cell contact, the oscillating field (0.3 Hz at 10 Gauss) was switched on for 10 s to quantify the elastic shear modulus (Pa/nm). (C) Junctional stiffness in wt versus ko cells in response to increasing applied shear stress. After 20 min of bead–cell contact, the field strength was increased stepwise in 10-s intervals with no pause between successive changes in the magnetic field. Each data point represents the mean. (D) The force-induced stiffening of Fc–E-cadherin–coated beads bound for 20 min to wt, ko, and vinculin-reconstituted F9 cells was measured using a modulated 0.3-Hz field (20 Gauss) for 50 s. (E, left) The mean intensity profile of vinculin IF plotted against the distance from the bead center for ∼80 unforced and forced beads. (right) Total vinculin intensity above baseline at unforced and forced beads measured in a 1-μm-wide area around the maximum of fluorescence intensity (gray). Error bars represent SD (A, triplicates; B–D, n > 300 [approximately one bead/cell]; E, n = ∼80).

did not increase after stimulation by HGF (unpublished data). It is possible that the low levels of vinculin that interact with E-cadherin, or the cross-linking method used, preclude the detection of changes in the complex. Alternatively, E-cadherin–vinculin complexes may form before translocation to cell–cell junctions.

Finally, we measured fluorescence resonance energy transfer (FRET) between vinculin and cell–cell junction complex members by means of acceptor photobleaching (see Materials and methods; Fig. S3). GFP-vinculin–expressing cells, stimulated for 1 h with HGF, were extracted in cytoskeleton-preserving (CSK) buffer, fixed, and stained for vinculin as donor (Alexa Fluor 488) and β-catenin or occludin as acceptor (rhodamine). Clear colocalization was found between vinculin and β-catenin at cell–cell junctions, whereas vinculin and occludin colocalized less often. FRET was measured in regions of colocalization. Higher FRET values were found for vinculin and β-catenin compared with vinculin and occludin (Fig. 3 D, left). This difference does not reflect a difference in acceptor concentration because regions were chosen with equal levels of acceptor as judged by rhodamine intensity (Fig. 3 D, right). The close proximity of vinculin to β-catenin suggests a specific association with the E-cadherin complex at cell–cell junctions.

Mutating alanine 50 to isoleucine resulted in a strong loss of vinculin's localization to cell–cell junctions and to integrin-dependent FAs (Fig. 3 E). This indicates that vinculin associates with the E-cadherin complex through mechanistically conserved interactions in its head domain (Bakolitsa et al., 2004). Whether β-catenin is the main recruiter of vinculin, as previously described in a different cell type (Peng et al., 2010), remains to be investigated.

Vinculin potentiates mechanosensing by the E-cadherin complex

To investigate the functional importance of vinculin for E-cadherin adhesion, we determined the adhesion of a panel of F9 cells (Xu et al., 1998) to E-cadherin–COMP. Vinculin knockout (ko) F9 cells showed reduced adhesion to E-cadherin–COMP when compared with wild-type (wt) F9 cells or vinculin ko F9 cells reconstituted with chicken vinculin (Fig. 4 A). This difference is because of impaired cell spreading, as indicated by the morphology of the few ko cells that remained bound to E-cadherin–COMP (Fig. 4 A, right). Functional E-cadherin was present at the plasma membrane because Fc–E-cadherin–coated beads readily adhered to the ko F9 cells (Fig. 4 B). Thus, vinculin is needed to form E-cadherin–dependent adhesive contacts that can support cell spreading.

This suggests that mechanical force is a principal conduit through which vinculin regulates E-cadherin adhesion. We further tested this using MTC. In Fig. 4 B, the force-independent increases in the local stiffness around E-cadherin–coated beads were similar for wt and ko F9 cells, indicating that basal E-cadherin adhesion is not affected by vinculin. In contrast, the stiffness increase in proportion to the applied force was clearly reduced in ko cells (Fig. 4 C). Furthermore,

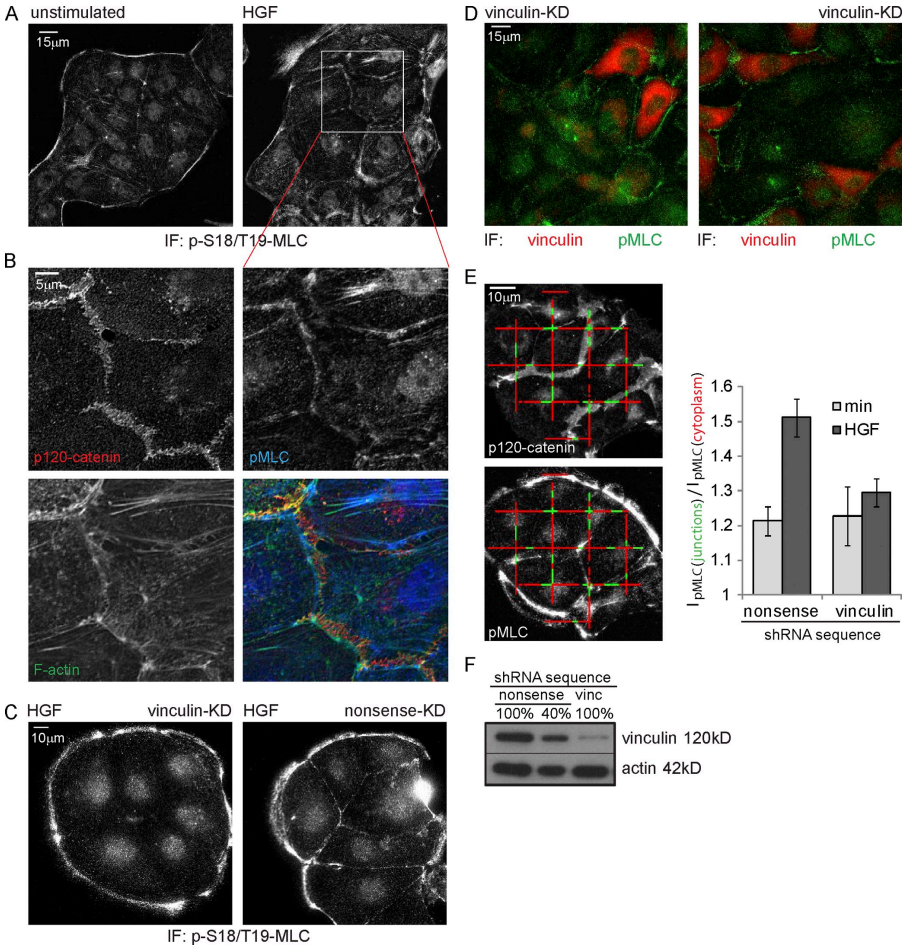

Figure 5. **Vinculin knockdown prevents HGF-induced pMLC accumulation near cell–cell junctions.** (A) HGF (2 h) induced increase in pMLC near cell–cell junctions revealed by IF. (B) A magnified view of A, showing that pMLC accumulates at F-actin structures that connect to p120-labeled cell–cell junctions. (C) IF shows a reduction of pMLC recruited to cell–cell junctions in vinculin knockdown (KD) cells after 2 h of HGF. (D) Overlay of the vinculin channel (smoothed with a Gaussian; $r = 40$) and pMLC channel of a dual-color IF staining of vinculin knockdown cells after 2 h of HGF. (E, left) Representative image automatically generated by custom software, displaying the line fragments used to measure pMLC levels near cell–cell junctions (green) and in the cytoplasm (red). (right) The relative intensity of pMLC near cell–cell junctions (a value of 1 means equal levels) shows an increase after 2 h of HGF that is largely abolished by vinculin knockdown. Error bars represent SEM. 25 images were analyzed for each condition.

ko cells displayed an ∼50% reduction in force-dependent reinforcement of cadherin junctions, which was fully restored by reconstitution with chicken vinculin (Fig. 4 D). Thus, loss of vinculin significantly reduces the mechanoresponse by the E-cadherin complex.

By immunofluorescence (IF), we noticed that vinculin and F-actin are already recruited to unforced beads. For quantification, we measured the fluorescence intensity at an increasing radius from the bead center, which was normalized to the peak level for each bead so that background levels, instead of peak intensity levels, vary. As shown in Fig. 4 E, the vinculin signal condenses around beads upon force. Furthermore, the intensity of vinculin (the curve area above background at 1-µm width around the intensity peak; Fig. 4 E, gray) slightly increases upon force. Clearly, this situation is quite different from the situation at intercellular junctions, where we observed de novo recruitment of vinculin. It is possible that the vinculin levels around unforced beads represent the buildup of intrinsic contractile actomyosin around larger beads (Choquet et al., 1997). Indeed, there was no evidence of either actin or vinculin accumulation near smaller E-cadherin–coated beads (Perez et al., 2008). In conclusion, these data show that vinculin potentiates the E-cadherin mechanoresponse concurrent with its strong increase at intercellular junctions, which experience increased tension, and with a moderate increase around forced beads.

Vinculin mediates the recruitment of active myosin to cell–cell junctions

We have previously shown that HGF signaling increases the presence of active myosin II (phosphorylated myosin light chain [pMLC]) in areas of cell–cell adhesion (de Rooij et al., 2005). A closer inspection of Fig. 5 B reveals that pMLC is present at F-actin structures that are just adjacent to cell–cell junctions and connect to the E-cadherin complex through thin actin bundles. As we show in Fig. 2, inhibition of myosin activity results in a loss of these actin-connected, vinculin-containing junctions. Conversely, we now investigated whether a loss of vinculin would affect these contractile actomyosin structures connected to cell–cell junctions. An ∼90% knockdown of vinculin (Fig. 5 F) resulted in a strong reduction in vinculin levels in the cytoplasm but did not completely deplete vinculin from FAs or intercellular junctions in MDCK cells. Although depletion of vinculin from cell–cell junctions was not complete, we observed a significant effect on the reorganization of junctions in response to HGF, which resulted in a strong loss of pMLC recruitment to cell–cell adhesions (Fig. 5 C). Fig. 5 D shows that this loss is specific for cells with a strongly reduced amount of vinculin. To quantify this, we used custom software that automatically divides the pixel intensity of the pMLC image in areas of cell–cell adhesion (Fig. 5 E, $I_{pMLC(junctions)}$, green) by the pixel intensity of the pMLC signal in the cytoplasm (Fig. 5 E, $I_{pMLC(cytoplasm)}$, red). As shown in Fig. 5 E, there is a strong reduction of the HGF-induced recruitment of

pMLC to cell–cell junctions in vinculin knockdown cells. Thus, we conclude that the recruitment of vinculin to active cell–cell junctions upon HGF is important for the remodeling of the cytoskeleton that connects to these junctions.

In conclusion, our nanomechanical experiments show that the E-cadherin complex is a bona fide mechanosensor. Furthermore, we uncover a novel role for vinculin in modulating E-cadherin–cytoskeleton mechanics and force-induced remodeling of cell–cell junctions. Because stiffness measured by MTC is a complex process, it is impossible to pinpoint the exact molecular mechanism that explains vinculin's role in E-cadherin mechanoregulation from these experiments. It is tempting to speculate similarity to integrin adhesion, but the molecules involved in vinculin recruitment to integrin adhesions (talin and paxillin) are not present at cell–cell contacts. Moreover, the proposed integrin mechanism (vinculin recruitment to stretched talin) would predict full inhibition of mechanosensing in the absence of vinculin, whereas we measure only partial inhibition. Furthermore, our MTC measurements show a strong effect on the stress–strain relation for E-cadherin junctions (Fig. 4 C), which is not found for integrin junctions (Mierke et al., 2008). All of this indicates that the mechanism of integrin-dependent force sensing may differ from mechanosensing at E-cadherin junctions. Thus, our data uncover a novel role for vinculin in E-cadherin mechanosensing, but, as for integrins, the exact mechanism remains to be established. Our findings have broad implications because of the central role of E-cadherin in the development and maintenance of epithelial tissues. Given the similarities in structure and binding characteristics among classical cadherins, it is tempting to speculate that cadherins may constitute a new family of tension sensors. The involvement of vinculin in cadherin mechanosensing and its localization to subdomains in activated cell–cell junctions opens the door for further investigations of molecular mechanisms underlying E-cadherin mechanoregulation.

Materials and methods

Cell lines and culture

MDCK and F9 cells were routinely cultured in high glucose DME (Invitrogen) supplemented with 10% FCS (Sigma-Aldrich) and penicillin/streptomycin (Invitrogen) in standard tissue culture dishes coated with 0.1% gelatin (Sigma-Aldrich) in the case of F9s. F9 ko cells were the γ229 cells, and chicken vinculin-reconstituted R16 cells were described previously (Xu et al., 1998). MDCK cell lines stably expressing EGFP- or mCherry-tagged constructs were generated by nucleofection (Lonza), G418 (Invitrogen) selection, and FACS sorting for intermediate levels of fluorescence. For imaging experiments, cells were grown on glass coverslips, glass-bottom dishes (WillCo Wells B.V.), or chamber coverslips (Thermo Fisher Scientific) coated with 10 µg/ml collagen type 1 (Sigma-Aldrich) or 20 µg/ml E-cadherin–COMP in medium supplemented with 0.5% FCS. 5 ng/ml HGF (Sigma-Aldrich) concentration was used.

Adhesion assays

Both MDCK cells and F9 cells were prepared by trypsinization from the culture dish, washed once in DME containing 10% FCS, incubated for 1 h under rotation in suspension in DME plus 10% FCS at 37°C, pelleted, and resuspended at the appropriate concentration in DME containing 0.5% FCS. MDCK adhesion assays were performed in 48-well plates coated with 20 µg/ml E-cadherin–COMP at a concentration of 100,000 cells per well. F9 cell adhesion was in 96-well plates coated with 20 µg/ml E-cadherin–COMP at a concentration of 100,000 cells per well. Adhesion was allowed for 45 min followed by three steps of rigorous washing in PBS supplemented with 1 mM $CaCl_2$ and quantified by measuring acid phosphatase activity (de Rooij et al., 2005).

Immunocytochemistry and microscopy

For immunocytochemistry, cells were washed three times in PBS (containing 1 mM $CaCl_2$ in the case of growth on E-cadherin–COMP) and fixed using 4% paraformaldehyde in PBS. Alternatively, if indicated, cells were washed two times for 1 min in CSK buffer (300 mM sucrose, 0.5% TX-100, 10 mM Pipes, pH 7, 50 mM NaCl, 3 mM $CaCl_2$, and 2 mM $MgCl_2$) before fixation. Live cell imaging, E-cadherin–COMP IF, and the colocalization imaging of α-catenin and EPLIN in Fig. S2 were performed on a microscope (Ti; Nikon) in a climate-controlled culture chamber using a 60× 1.49 NA Apo TIRF objective lens and an electron microscopy charge-coupled device camera (Luka; Andor). To image cell–cell junctions in Fig. 2 and Fig. S2, immunostained cells on collagen were imaged using a confocal microscope (TCS-SP2; Leica) with a 63× 1.32 NA objective lens and a pinhole setting of 1 airy disk. For FRET measurements, cells were imaged on a confocal microscope (TCS-SP5; Leica) with a 63× 1.32 NA objective lens using a four times zoom and a pinhole setting of 3 mm. Acceptor photobleaching was achieved by scanning the central area of the image with a 20 times zoom using a 561 laser at full power. All widefield images, unless specifically indicated otherwise, and with the exception of the E-cadherin–COMP images in Fig. 3 B and Fig. 2 (A and F), were sharpened for display with an unsharp mask filter in ImageJ (National Institutes of Health; r = 3; weight = 0.6) and background subtracted by rolling ball (r = 40).

Quantification of fluorescence imaging

To measure the decay of vinculin from cell–cell junctions and FAs after inhibition of actomyosin contractility, we cleaned up the time-lapse image series using the unsharp mask filter and background subtraction. Regions of interest (ROIs) were drawn that encompassed two to four closely grouped FAs or a vinculin-containing area of cell–cell adhesion. The decay in each of these ROIs was corrected for bleaching and fluctuations by neighboring background ROIs and normalized between 0 (background level at the end of the curve) and 1 (mean vinculin ROI intensity before addition of inhibitors). Normalized intensities from individual ROIs were averaged per frame and displayed in Fig. 2 C.

To quantify changes in pMLC intensity at cell–cell junctions, a custom function was written in MATLAB (MathWorks) that draws a grid of 9-pixel-wide horizontal and vertical lines on the images, which were first flattened by background subtraction. These lines are spaced 170 pixels apart and from the edges of the image. Thresholding was used to determine the edges of cell islands, and lines were shortened to end at least 100 pixels from these edges (on the inside of the island) or from the edge of the image (Fig. 5 E, red). Peaks in pixel intensity in the p120-catenin image were used to automatically define the location of cell–cell junctions along these lines and mark 60-pixel fragments on the lines that span peaks (Fig. 5 E, green). Pixel intensities along these line fragments in the pMLC image were divided by pixel intensities along the rest of the red lines to calculate the relative pMLC levels near cell–cell junctions.

Acceptor photobleaching (FRET)

FRET efficiencies were measured by acceptor photobleaching. Donor (GFP-vinculin stained by anti-GFP with Alexa Fluor 488–labeled secondary antibodies) and acceptor (indicated primary with rhodamine-labeled secondary antibodies) confocal images were collected before and after photobleaching of the acceptor in a defined region of the image (Fig. S3). Laser, microscope, and scanhead settings were identical throughout these experiments, and the images were corrected for background and nonspecific bleaching during scanning. The FRET values were calculated from the mean fluorescent values from ROIs. Three to five ROIs comprising cell–cell junctions outside the bleach area were used to calculate bleaching caused by imaging, and three to five ROIs inside the bleach area were used to calculate the percent loss in acceptor fluorescence and the gain in donor fluorescence upon acceptor bleaching. The postbleach donor values were corrected for acceptor photo conversion. Photo conversion of the acceptor was measured by imaging in 20 ROIs in five independent images of cells that were stained only with acceptor antibodies (β-catenin + anti–mouse rhodamine) and determined to be 1.12 ± 0.3%. The donor fluorescence loss in the prebleach donor image was calculated by subtracting the prebleach donor image from the corrected postbleach donor image and dividing this by the fraction of acceptor bleaching to correct for incomplete acceptor bleaching (in all experiments >0.8). The FRET percent was calculated by relating the donor fluorescence loss in the prebleach donor image to the total donor fluorescence (prebleach donor image plus donor fluorescence loss in the prebleach donor image).

Antibodies and DNA constructs

Mouse monoclonal vinculin antibody (hVin-1) and rabbit polyclonal α-catenin antibody were obtained from Sigma-Aldrich. Mouse monoclonal

E-cadherin (clones 36 and 34), β- and p120-catenin, paxillin, and EPLIN antibodies were obtained from BD. Polyclonal pMLC antibody (pS18/T19) was obtained from Cell Signaling Technology. Mouse monoclonal occludin antibody was obtained from Invitrogen. Alexa Fluor 488 phalloidin and Alexa Fluor 488, Alexa Fluor 594, or Texas red–labeled secondary antibodies were obtained from Invitrogen. The EGFP–E-cadherin construct was provided by A. Kusumi (Japan Science and Technology Corporation, Chiyoda, Nagoya, Japan; Iino et al., 2001). Chicken vinculin was cloned in the pEGFP-C3 vector, resulting in expression of full-length N-terminal EGFP-tagged vinculin. Murine p120-catenin was cloned in the mCherry-N1 vector (identical to pEGFP-N1, with EGFP replaced by mCherry) to express full-length C-terminal mCherry-tagged p120-catenin. pEGFP-N1-paxillin was provided by M.H. Ginsberg (University of California, San Diego, La Jolla, CA; Nishiya et al., 2005) and was cloned into the mCherry-N1 vector. EGFP-nectin1 was provided by C. Krummenacher (University of Pennsylvania, Philadelphia, PA; Krummenacher et al., 2003), GFP-claudin3 was provided by M. Furuse (Jichi Medical University, Shimotsuke, Tochigi, Japan; Matsuda et al., 2004), and vinculin A50I was provided by C. Ballestrem (University of Manchester, Manchester, England, UK). Vinculin knockdown was performed by nucleofection of a mix of two pSuper vectors containing vinculin-directed shRNA inserts, 5′-AAGAGTTGCTGCCAGTTCTC-ATT-3′ and 5′-AAACCAAGGAATAGAAGAAGCTT-3′. Control (nonsense) knockdown used the identical procedure with a pSuper vector with none-coding insert.

E-cadherin–COMP expression and purification

The E-cadherin–COMP-His6 expression construct was provided by O. Pertz (University of Basel, Basel, Switzerland; Pertz et al., 1999). Expression was performed by transient transfection in HEK293T cells followed by culturing for 2 d on low serum medium and Ni-NTA affinity purification of the secreted E-cadherin–COMP-His6 from the culture medium.

IP

Cells were grown for 24 h on 3 µg/ml collagen-coated tissue culture dishes in DME supplemented with 0.5% FCS (HGF was added for 2 h when indicated) or for 14 h in 60 µM $CaCl_2$ containing EpiLife followed by 1 h addition of up to 1.8 mM $CaCl_2$. Cells were washed twice with PBS containing 1 mM $CaCl_2$ at RT before adding 3 ml PBS with 1 mM $CaCl_2$ containing 200 µg/ml DSP (DSP prepared as 100× stock in DMSO diluted immediately before use) per 10-cm dish. Next, cells were incubated on a rocking platform for 20 min at RT and washed twice with PBS at RT before washing four times with ice-cold quenching buffer (10 mM Tris, pH 7.5, in PBS). Excess liquid was removed, and cells were scraped in 800 µl of ice-cold lysis buffer (25 mM Tris, pH 7.5, 1% NP-40, 1% deoxycholic acid, 150 mM NaCl, protease inhibitor cocktail (1:1000; Roche), 10 µl/ml leupeptin, 1 mM sodium fluoride, and 1 mM sodium orthovanadate). The lysate was spun at 4°C for 10 min at 16,100 relative centrifugal force, the supernatant was removed, and the pellet was triturated in 100 µl SDS-IP buffer (15 mM Tris, pH 7.5, 5 mM EDTA, 2.5 mM EGTA, and 1% SDS) by use of a 23-G needle and subsequently a 29-G insulin needle. The sample was put at 100°C for 10 min, diluted with 900 µl of lysis buffer, and spun at 4°C for 10 min at 16,100 relative centrifugal force. Supernatant was added to protein A–Sepharose beads (GE Healthcare) precoupled with GFP antibody (custom-made rabbit polyclonal) and incubated for 2 h at 4°C. The beads were washed four times with cold lysis buffer and remnant liquid was removed and boiled for 10 min in 50 µl of Laemmli sample buffer (containing 5% β-mercaptoethanol). Samples were run on a 4–12% gradient SDS-PAGE gel (NuPage; Invitrogen), blotted onto PVDF membranes, and analyzed with the indicated primary antibodies followed by HRP-coupled secondary antibodies and ECL detection. Monoclonal E-cadherin (clone 36), monoclonal paxillin, and monoclonal β-catenin were obtained from BD. Polyclonal vinculin (hVin-1) was obtained from Sigma-Aldrich.

MTC

MTC measurements were performed with a home-built instrument. F9 cells were cultured on mixed laminin/poly-L-lysine substrates and grown to confluence. 4.5-µm ferromagnetic beads (Spherotech) were covalently modified with Fc-tagged human E-cadherin. The latter recombinant protein (Niessen and Gumbiner, 2002) was expressed by stably transfected CHO cells cultured in DME containing 10% FBS and 0.4 mg/ml geneticin. During the protein collection phase, the culture medium was switched to serum-free DME to simplify the purification and increase protein yields. Fc–E-cadherin was purified from the serum-free conditioned medium on a protein A affinity column (Affigel; Bio-Rad Laboratories; Prakasam et al., 2006b). Before immobilization, the carboxyl groups on the beads were activated with ethyl-3-(dimethylaminopropyl)-carbodiimide/*N*-hydroxysuccinimide treatment (Prakasam et al., 2006a,b). Incubating the activated beads with soluble E-cadherin covalently linked the protein to the beads. Alternatively, beads were labeled with monoclonal anti–E-cadherin antibodies (also used as a blocking antibody in these experiments; clone 34; BD) using an identical protocol. The E-cadherin–coated beads were incubated with a confluent cell monolayer on a heated microscope stage at 37°C. All MTC imaging was performed on an inverted microscope (Leica) using a 20× 0.6 NA objective and a cooled charge-coupled device camera (Orca2; Hamamatsu Photonics). Control beads were similarly modified with poly-L-lysine. In all measurements, an initial, brief high field was applied to magnetize the beads. After defined time periods, the oscillating magnetic field perpendicular to the bead magnetic moment was turned on for a defined period to induce a modulating shear stress on the beads. Inhibitors in Fig. 1 were added 10 min before MTC measurements. EGTA was added just before MTC measurements. The bead magnetic moment constant was calibrated in a viscosity standard by rotating the beads in the fluid and measuring the bead angular strain (Wang et al., 1993), determined to be 0.12 Pa/Gauss magnetic field. The bead displacements were directly measured and converted to the complex modulus/stiffness by taking the ratio of the applied stress (bead magnetic moment constant × applied magnetic field) to the bead displacement (Wang et al., 1993). Fourier transforms of the bead displacements and the specific torque were used to determine the complex modulus of the bead–cell junction (Fabry et al., 2001). Decreases in the amplitude of bead displacements at a given torque reflect increases in local junction stiffness, which can arise from such processes as adhesion protein accumulation, mechanical reinforcement of the bonds, increased cell contractility, or actin reorganization. Force-independent changes could arise from processes such as E-cadherin accumulation at bead–cell contacts (Perez et al., 2008). Each measurement (experimental condition) represents measurements with $n > 300$ cells at approximately bead per cell. The data follow a log normal distribution from which we obtained the mean and standard deviation. The Student's *t* test was used to compare measurements, with $P < 0.05$ indicative of a statistically significant difference.

Quantification of vinculin around Fc–E-cadherin–coated beads

To investigate the effect of force on vinculin recruitment, the cells were incubated with beads and fixed without applying force or after force application. The cells were stained with either vinculin antibody or rhodamine-conjugated phalloidin. Imaging was performed on a microscope (200M; Carl Zeiss, Inc.) using a 100× 1.3 NA objective and a cooled charge-coupled device camera (AxioCam; Carl Zeiss, Inc.). For each cell-attached bead, the fluorescent image was divided into concentric rings centered at the bead center, and the mean fluorescent intensity was calculated at a different ring radius or position. This fluorescent intensity profile of each bead was subtracted by the background, normalized to its maximum, and averaged for ∼80 beads.

Online supplemental material

Fig. S1 shows localization of E-cadherin–actin linkers after HGF. Fig. S2 shows that E-cadherin–COMP adhesions are cadherin- and myosin II–dependent structures that contain the core E-cadherin complex. Fig. S3 further explains the FRET data shown in Fig. 3 D. Video 1 shows that vinculin is recruited to p120-catenin containing cell–cell junctions after HGF. Video 2 shows that the cell–cell junction pool of vinculin is distinct from the vinculin pool at the basal FAs and that they are both localized in an actomyosin-dependent manner. Video 3 shows that vinculin at cell–cell contacts does not overlap with paxillin-positive FAs. Online supplemental material is available at http://www.jcb.org/cgi/content/full/jcb.201001149/DC1.

We thank Eileen Adamson for the F9 cell lines and Jacco van Rheenen for advice on FRET.

This work was supported by The American Institute for Cancer Research (grant 06-0528), The Dutch Foundation for Cancer Research (KWF; grant 2006-3714 to J. de Rooij), and The National Institutes of Health (grant GM 072744 to N. Wang). D. Leckband was supported by The Reid T. Milner Professorship and The National Science Foundation (Chemical, Bioengineering, Environmental, and Transport Systems; grant 0853705).

Submitted: 27 January 2010
Accepted: 2 June 2010

References

Abe, K., and M. Takeichi. 2008. EPLIN mediates linkage of the cadherin catenin complex to F-actin and stabilizes the circumferential actin belt. *Proc. Natl. Acad. Sci. USA.* 105:13–19. doi:10.1073/pnas.0710504105

Avizienyte, E., V.J. Fincham, V.G. Brunton, and M.C. Frame. 2004. Src SH3/2 domain-mediated peripheral accumulation of Src and phospho-myosin is linked to deregulation of E-cadherin and the epithelial-mesenchymal transition. *Mol. Biol. Cell.* 15:2794–2803. doi:10.1091/mbc.E03-12-0879

Ayollo, D.V., I.Y. Zhitnyak, J.M. Vasiliev, and N.A. Gloushankova. 2009. Rearrangements of the actin cytoskeleton and E-cadherin-based adherens junctions caused by neoplasic transformation change cell-cell interactions. *PLoS One.* 4:e8027. doi:10.1371/journal.pone.0008027

Bakolitsa, C., D.M. Cohen, L.A. Bankston, A.A. Bobkov, G.W. Cadwell, L. Jennings, D.R. Critchley, S.W. Craig, and R.C. Liddington. 2004. Structural basis for vinculin activation at sites of cell adhesion. *Nature.* 430:583–586. doi:10.1038/nature02610

Bershadsky, A.D., N.Q. Balaban, and B. Geiger. 2003. Adhesion-dependent cell mechanosensitivity. *Annu. Rev. Cell Dev. Biol.* 19:677–695. doi:10.1146/annurev.cellbio.19.111301.153011

Choquet, D., D.P. Felsenfeld, and M.P. Sheetz. 1997. Extracellular matrix rigidity causes strengthening of integrin-cytoskeleton linkages. *Cell.* 88:39–48. doi:10.1016/S0092-8674(00)81856-5

de Rooij, J., A. Kerstens, G. Danuser, M.A. Schwartz, and C.M. Waterman-Storer. 2005. Integrin-dependent actomyosin contraction regulates epithelial cell scattering. *J. Cell Biol.* 171:153–164. doi:10.1083/jcb.200506152

del Rio, A., R. Perez-Jimenez, R. Liu, P. Roca-Cusachs, J.M. Fernandez, and M.P. Sheetz. 2009. Stretching single talin rod molecules activates vinculin binding. *Science.* 323:638–641. doi:10.1126/science.1162912

Discher, D.E., P. Janmey, and Y.L. Wang. 2005. Tissue cells feel and respond to the stiffness of their substrate. *Science.* 310:1139–1143. doi:10.1126/science.1116995

Drees, F., S. Pokutta, S. Yamada, W.J. Nelson, and W.I. Weis. 2005. Alpha-catenin is a molecular switch that binds E-cadherin-beta-catenin and regulates actin-filament assembly. *Cell.* 123:903–915. doi:10.1016/j.cell.2005.09.021

Fabry, B., G.N. Maksym, S.A. Shore, P.E. Moore, R.A. Panettieri Jr., J.P. Butler, and J.J. Fredberg. 2001. Selected contribution: time course and heterogeneity of contractile responses in cultured human airway smooth muscle cells. *J. Appl. Physiol.* 91:986–994.

Giannone, G., G. Jiang, D.H. Sutton, D.R. Critchley, and M.P. Sheetz. 2003. Talin1 is critical for force-dependent reinforcement of initial integrin–cytoskeleton bonds but not tyrosine kinase activation. *J. Cell Biol.* 163:409–419. doi:10.1083/jcb.200302001

Hazan, R.B., L. Kang, S. Roe, P.I. Borgen, and D.L. Rimm. 1997. Vinculin is associated with the E-cadherin adhesion complex. *J. Biol. Chem.* 272:32448–32453. doi:10.1074/jbc.272.51.32448

Hinck, L., I.S. Näthke, J. Papkoff, and W.J. Nelson. 1994. Dynamics of cadherin/catenin complex formation: novel protein interactions and pathways of complex assembly. *J. Cell Biol.* 125:1327–1340. doi:10.1083/jcb.125.6.1327

Humphries, J.D., P. Wang, C. Streuli, B. Geiger, M.J. Humphries, and C. Ballestrem. 2007. Vinculin controls focal adhesion formation by direct interactions with talin and actin. *J. Cell Biol.* 179:1043–1057. doi:10.1083/jcb.200703036

Iino, R., I. Koyama, and A. Kusumi. 2001. Single molecule imaging of green fluorescent proteins in living cells: E-cadherin forms oligomers on the free cell surface. *Biophys. J.* 80:2667–2677. doi:10.1016/S0006-3495(01)76236-4

Kardash, E., M. Reichman-Fried, J.L. Maître, B. Boldajipour, E. Papusheva, E.M. Messerschmidt, C.P. Heisenberg, and E. Raz. 2010. A role for Rho GTPases and cell-cell adhesion in single-cell motility in vivo. *Nat. Cell Biol.* 12:47–53: 1–11. doi:10.1038/ncb2003

Krendel, M., N.A. Gloushankova, E.M. Bonder, H.H. Feder, J.M. Vasiliev, and I.M. Gelfand. 1999. Myosin-dependent contractile activity of the actin cytoskeleton modulates the spatial organization of cell-cell contacts in cultured epitheliocytes. *Proc. Natl. Acad. Sci. USA.* 96:9666–9670. doi:10.1073/pnas.96.17.9666

Krummenacher, C., I. Baribaud, R.J. Eisenberg, and G.H. Cohen. 2003. Cellular localization of nectin-1 and glycoprotein D during herpes simplex virus infection. *J. Virol.* 77:8985–8999. doi:10.1128/JVI.77.16.8985-8999.2003

Kumar, S., and V.M. Weaver. 2009. Mechanics, malignancy, and metastasis: the force journey of a tumor cell. *Cancer Metastasis Rev.* 28:113–127. doi:10.1007/s10555-008-9173-4

Lambert, M., O. Thoumine, J. Brevier, D. Choquet, D. Riveline, and R.M. Mège. 2007. Nucleation and growth of cadherin adhesions. *Exp. Cell Res.* 313:4025–4040. doi:10.1016/j.yexcr.2007.07.035

Lecuit, T. 2005. Adhesion remodeling underlying tissue morphogenesis. *Trends Cell Biol.* 15:34–42. doi:10.1016/j.tcb.2004.11.007

Lecuit, T., and P.F. Lenne. 2007. Cell surface mechanics and the control of cell shape, tissue patterns and morphogenesis. *Nat. Rev. Mol. Cell Biol.* 8:633–644. doi:10.1038/nrm2222

Maddugoda, M.P., M.S. Crampton, A.M. Shewan, and A.S. Yap. 2007. Myosin VI and vinculin cooperate during the morphogenesis of cadherin cell–cell contacts in mammalian epithelial cells. *J. Cell Biol.* 178:529–540. doi:10.1083/jcb.200612042

Matsuda, M., A. Kubo, M. Furuse, and S. Tsukita. 2004. A peculiar internalization of claudins, tight junction-specific adhesion molecules, during the intercellular movement of epithelial cells. *J. Cell Sci.* 117:1247–1257. doi:10.1242/jcs.00972

Mierke, C.T., P. Kollmannsberger, D.P. Zitterbart, J. Smith, B. Fabry, and W.H. Goldmann. 2008. Mechano-coupling and regulation of contractility by the vinculin tail domain. *Biophys. J.* 94:661–670. doi:10.1529/biophysj.107.108472

Miyake, Y., N. Inoue, K. Nishimura, N. Kinoshita, H. Hosoya, and S. Yonemura. 2006. Actomyosin tension is required for correct recruitment of adherens junction components and zonula occludens formation. *Exp. Cell Res.* 312:1637–1650. doi:10.1016/j.yexcr.2006.01.031

Niessen, C.M., and B.M. Gumbiner. 2002. Cadherin-mediated cell sorting not determined by binding or adhesion specificity. *J. Cell Biol.* 156:389–399. doi:10.1083/jcb.200108040

Nishiya, N., W.B. Kiosses, J. Han, and M.H. Ginsberg. 2005. An alpha4 integrin-paxillin-Arf-GAP complex restricts Rac activation to the leading edge of migrating cells. *Nat. Cell Biol.* 7:343–352. doi:10.1038/ncb1234

Pasapera, A.M., I.C. Schneider, E. Rericha, D.D. Schlaepfer, and C.M. Waterman. 2010. Myosin II activity regulates vinculin recruitment to focal adhesions through FAK-mediated paxillin phosphorylation. *J. Cell Biol.* 188:877–890. doi:10.1083/jcb.200906012

Peng, X., L.E. Cuff, C.D. Lawton, and K.A. DeMali. 2010. Vinculin regulates cell-surface E-cadherin expression by binding to beta-catenin. *J. Cell Sci.* 123:567–577. doi:10.1242/jcs.056432

Perez, T.D., M. Tamada, M.P. Sheetz, and W.J. Nelson. 2008. Immediate-early signaling induced by E-cadherin engagement and adhesion. *J. Biol. Chem.* 283:5014–5022. doi:10.1074/jbc.M705209200

Pertz, O., D. Bozic, A.W. Koch, C. Fauser, A. Brancaccio, and J. Engel. 1999. A new crystal structure, Ca2+ dependence and mutational analysis reveal molecular details of E-cadherin homoassociation. *EMBO J.* 18:1738–1747. doi:10.1093/emboj/18.7.1738

Prakasam, A., Y.H. Chien, V. Maruthamuthu, and D.E. Leckband. 2006a. Calcium site mutations in cadherin: impact on adhesion and evidence of cooperativity. *Biochemistry.* 45:6930–6939. doi:10.1021/bi060213m

Prakasam, A.K., V. Maruthamuthu, and D.E. Leckband. 2006b. Similarities between heterophilic and homophilic cadherin adhesion. *Proc. Natl. Acad. Sci. USA.* 103:15434–15439. doi:10.1073/pnas.0606701103

Schwartz, M.A., and D.W. DeSimone. 2008. Cell adhesion receptors in mechanotransduction. *Curr. Opin. Cell Biol.* 20:551–556. doi:10.1016/j.ceb.2008.05.005

Shewan, A.M., M. Maddugoda, A. Kraemer, S.J. Stehbens, S. Verma, E.M. Kovacs, and A.S. Yap. 2005. Myosin 2 is a key Rho kinase target necessary for the local concentration of E-cadherin at cell-cell contacts. *Mol. Biol. Cell.* 16:4531–4542. doi:10.1091/mbc.E05-04-0330

Tomschy, A., C. Fauser, R. Landwehr, and J. Engel. 1996. Homophilic adhesion of E-cadherin occurs by a co-operative two-step interaction of N-terminal domains. *EMBO J.* 15:3507–3514.

Tzima, E., M. Irani-Tehrani, W.B. Kiosses, E. Dejana, D.A. Schultz, B. Engelhardt, G. Cao, H. DeLisser, and M.A. Schwartz. 2005. A mechanosensory complex that mediates the endothelial cell response to fluid shear stress. *Nature.* 437:426–431. doi:10.1038/nature03952

Vogel, V., and M. Sheetz. 2006. Local force and geometry sensing regulate cell functions. *Nat. Rev. Mol. Cell Biol.* 7:265–275. doi:10.1038/nrm1890

Wang, N., and D.E. Ingber. 1995. Probing transmembrane mechanical coupling and cytomechanics using magnetic twisting cytometry. *Biochem. Cell Biol.* 73:327–335. doi:10.1139/o95-041

Wang, N., J.P. Butler, and D.E. Ingber. 1993. Mechanotransduction across the cell surface and through the cytoskeleton. *Science.* 260:1124–1127. doi:10.1126/science.7684161

Xu, W., J.L. Coll, and E.D. Adamson. 1998. Rescue of the mutant phenotype by reexpression of full-length vinculin in null F9 cells; effects on cell locomotion by domain deleted vinculin. *J. Cell Sci.* 111:1535–1544.

Yamada, S., S. Pokutta, F. Drees, W.I. Weis, and W.J. Nelson. 2005. Deconstructing the cadherin-catenin-actin complex. *Cell.* 123:889–901. doi:10.1016/j.cell.2005.09.020

Zhong, C., M.S. Kinch, and K. Burridge. 1997. Rho-stimulated contractility contributes to the fibroblastic phenotype of Ras-transformed epithelial cells. *Mol. Biol. Cell.* 8:2329–2344.